Fluid Dynamics Research 8 (1991) 1–8
North-Holland

FLUID DYNAMICS
RESEARCH

Direct simulation of three-dimensional turbulence in the Taylor–Green vortex

M.E. Brachet

Laboratoire de Physique Statistique, CNRS, Ecole Normale Supérieure, 24 rue Lhomond, 75231 Paris Cedex 05, France

Received 1 February 1991; revised manuscript received 30 May 1991

Abstract. The incompressible Navier–Stokes equations are numerically integrated on a Cray-2 machine with the periodic Taylor–Green initial data. Using a spectral method taking advantage of the symmetries of the flow, a resolution of 864^3 and corresponding high Reynolds numbers ($R_\lambda = 140$) are obtained Visualisations of the resulting turbulent flow show that the turbulent activity is strongly correlated with low-pressure zones. We demonstrate that this behavior of the pressure field is linked to the fact that the square vorticity is spatially more concentrated than the energy dissipation.

Turbulence is said to be developed when the scales transporting energy and those in which dissipation occurs are widely separated. This necessitates integral-scale Reynolds numbers that are at least on the order of several thousand (or Taylor microscale based Reynolds number R_λ of at least a hundred). Much higher Reynolds numbers are obtained experimentally. Nevertheless, the current experimental methods measure only the velocity, and thus knowledge of the small-scale structures characterized by large velocity gradients remains fragmentary [1]. To study developed turbulence numerically, a large range of spatial scales, and hence high resolution, is essential. One is quickly limited by the computer's size. An idea that comes to mind is to simplify the geometry of the flow, for example by using periodic boundary conditions [2].

The Taylor–Green vortex [3] is the three-dimensional flow that develops, following the constant density incompressible Navier–Stokes equations,

$$\partial_t \boldsymbol{v} + (\boldsymbol{v}\cdot\nabla)\boldsymbol{v} = -1/\rho\,\nabla p + \nu\,\Delta v,$$

with periodic boundary conditions, from the initial data:

$$v_x = \sin(x)\cos(y)\cos(z), \quad v_y = -\cos(x)\sin(y)\cos(z), \quad v_z = 0.$$

This is perhaps the simplest system in which to study the generation of excitation at small scales and the resulting turbulence. Since the initial conditions are products of trigonometric functions, we can use spectral methods, which are both simple to implement and accurate [4].

Compared to flows which are simply periodic, the Taylor–Green vortex displays additional symmetries. By taking advantage of these additional symmetries in the spectral integration algorithm for the Navier–Stokes equations, it is possible to gain factors of 64 in memory, of 32 in number of operations, and thus a factor of 4 in the separation of scales for a given computational power. In practice it is possible to run incore on a 256 Mbyte, 4-processor Cray-2 machine with a resolution of 864^3 (at the cost of tens of CPU hours per turnover time).

The evolution at large Reynolds numbers of the Taylor–Green vortex follows essentially two phases [5]. During the first phase, the viscous effects can be neglected, and small-scale

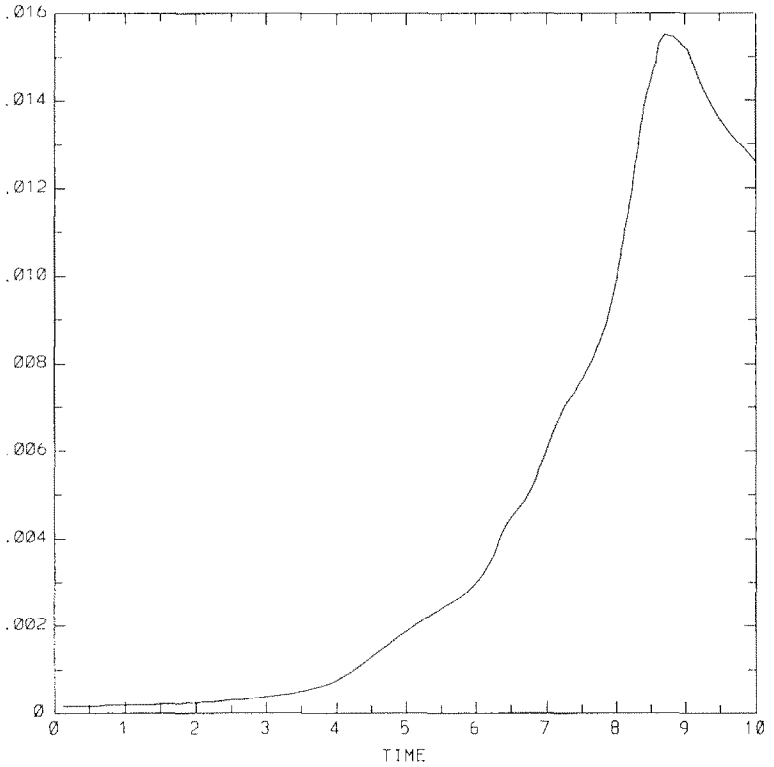

Fig. 1. Energy dissipation per unit mass $\epsilon(t) = \nu \int d\boldsymbol{r} \frac{1}{2} \sum_{i,j} (\partial_i v_j + \partial_j v_i)^2$ versus time. The maximum is reached, after a few eddy turnover times, around $t = 9$.

structures are generated which are well-organized and laminar. During the second phase, viscous diffusion plays an important role in the dynamics and distordered dissipative structures are created. The energy dissipation attains its maximum at a late stage of the viscous phase. In the simulation which we present here, with a resolution of 864^3 and with a Reynolds number (defined as the inverse of the kinematic viscosity) of 5000, this maximum takes place at $t = 9$ (see fig. 1). Figure 2 shows the energy spectrum, defined here as the kinetic energy per unit volume and per wavenumber (averaged over angle) at the moment of the maximum of the energy dissipation. Note that, over more than a decade, an inertial range is present over which the spectrum follows a power law with exponent close to the value of $-5/3$ predicted by Kolmogorov [6], followed by a dissipative zone. At this instant in time, the Reynolds number R_λ defined using the Taylor microscale is about 140.

The chaotic and highly intermittent appearance of the small-scale excitations is shown in fig. 3 which represents, in a planar section at $y = \pi/4$, the square of vorticity

$$\omega^2 = (\nabla \times \boldsymbol{v})^2 \quad \text{or} \quad \omega^2 = \tfrac{1}{2} \sum_{ij} (\partial_i v_j - \partial_j v_i)^2.$$

Figure 4 represents in the same fashion the local energy dissipation $\rho \nu \sigma^2$ where

$$\sigma^2 = \tfrac{1}{2} \sum_{ij} (\partial_i v_j + \partial_j v_i)^2.$$

Note that the energy dissipation appears to look somewhat less spatially concentrated than the square of vorticity.

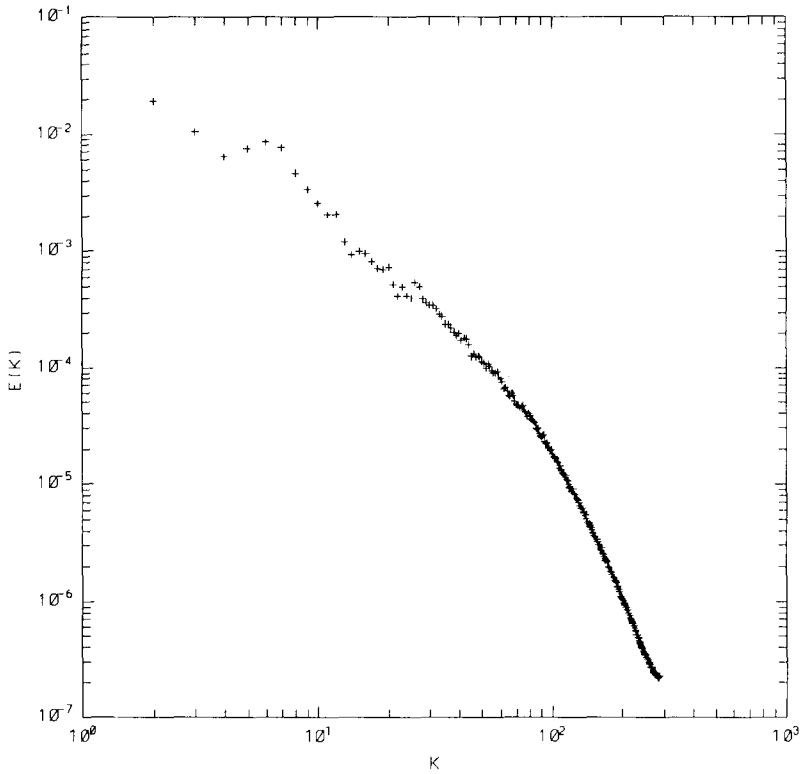

Fig. 2. Energy spectrum $E(k)$ at $t = 9$. Note that the slope is close to Kolmogorov's value $-5/3$ beteween $k = 6$ and $k = 60$.

There is a simple equation that relates the pressure field to the square vorticity and the energy dissipation fields. Indeed, by taking the divergence of the Navier–Stokes equations, in a constant density incompressible fluid, we find

$$2\Delta p/\rho + \sigma^2 - \omega^2 = 0.$$

It is therefore natural to establish an *analogy to electrostatics, with the pressure corresponding to the potential resulting from negative and positive charges distributed according to the square vorticity and the energy dissipation, respectively.* The vorticity concentrations thus act like sources of low pressure and their greatest relative concentration relatively to the energy dissipation concentrations acting as source of high-pressure will be the cause of spatial correlation between turbulent activity and low-pressure regions. This is confirmed by looking at fig. 5, which represents the pressure field p. Figure 5 shows that the zones of turbulent activity are correlated with the low-pressure regions. These regions appear to be point-like on the 2D cut. By looking at other cuts (data not shown) one can see the low-pressure regions to be extended in the third dimension, i.e. they are in fact filaments.

The simple picture that now emerges is thus that the regions of high square vorticity are distributed on structures that are rather tube-like while the regions of high energy dissipation are distributed on structures that are rather sheet-like. As a consequence strong depressions are observed on the tubes, while milder high-pressures are seen on the sheets. The flow seems to be organized around the low-pressure high-vorticity filaments, e.g., see fig. 6 which displays the magnitude of the velocity field and shows that sheet-like high velocity regions are wrapped around the filaments.

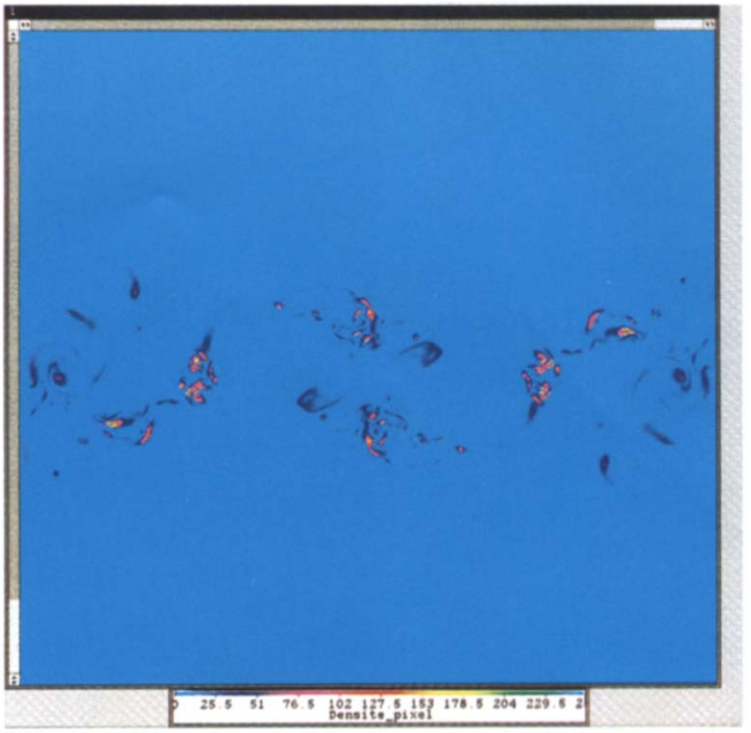

Fig. 3. Raster visualisation of square vorticity $\omega^2 = \frac{1}{2}\Sigma_{ij}(\partial_i v_j - \partial_j v_i)^2$ in the plane $y = \pi/4$ at $t = 9$. Because of the symmetries, only the aera $0 < x < \pi$, $0 < z < \pi$ is shown. The colormap we chose displays the high-vorticity regions in dark.

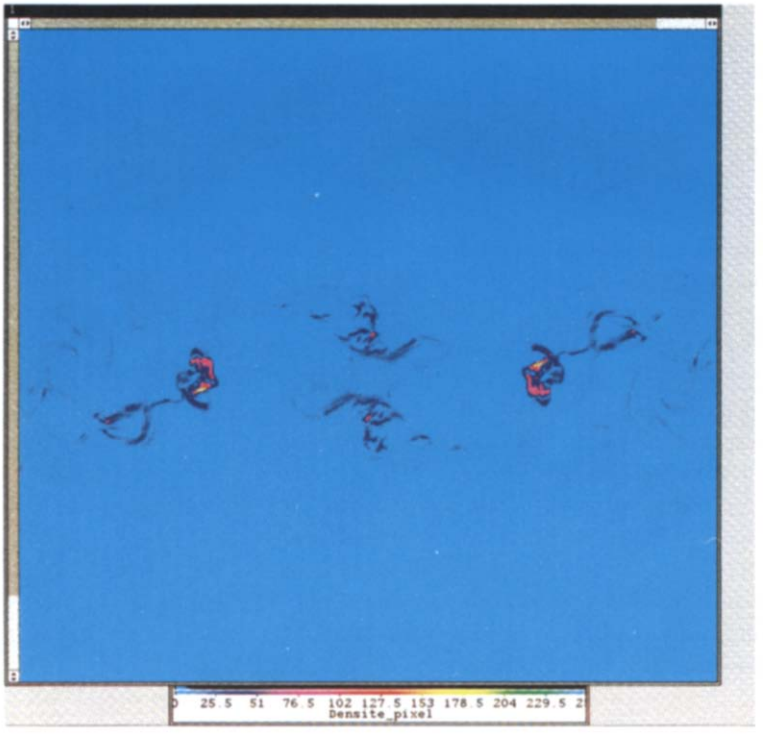

Fig. 4. Raster visualisation, at $t = 9$ and in the same aera as in fig. 3, of the normalized energy dissipation field $\sigma^2 = \frac{1}{2}\Sigma_{ij}(\partial_i v_j + \partial_j v_i)^2$ in the plane $y = \pi/4$. The colormap is the same as in fig. 3.

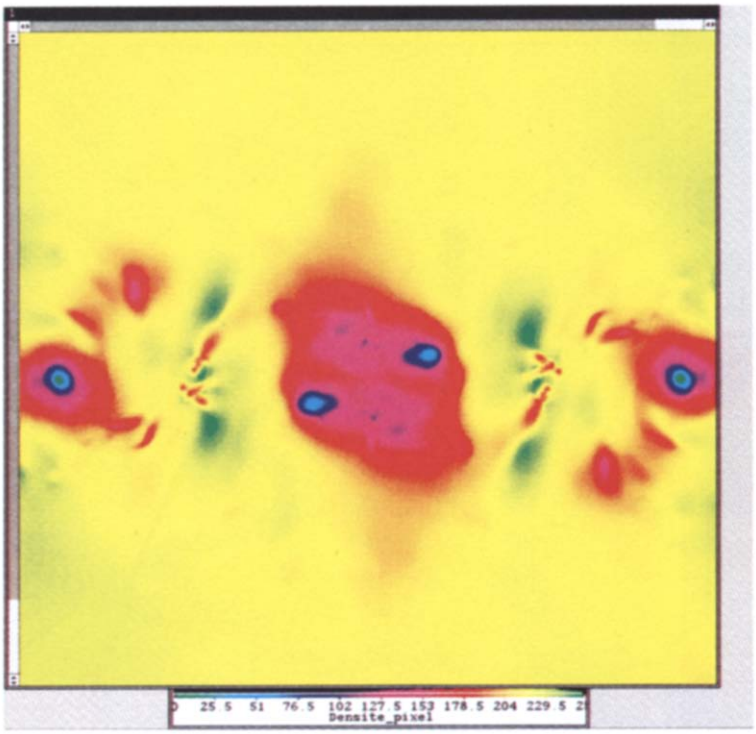

Fig. 5. Raster visualisation of the pressure field in the plane $y = \pi/4$ at $t = 9$, shown as in figs. 3 and 4. Note the sharp pressure minimum indicating the crossing of the figure's plane by a vortex filament.

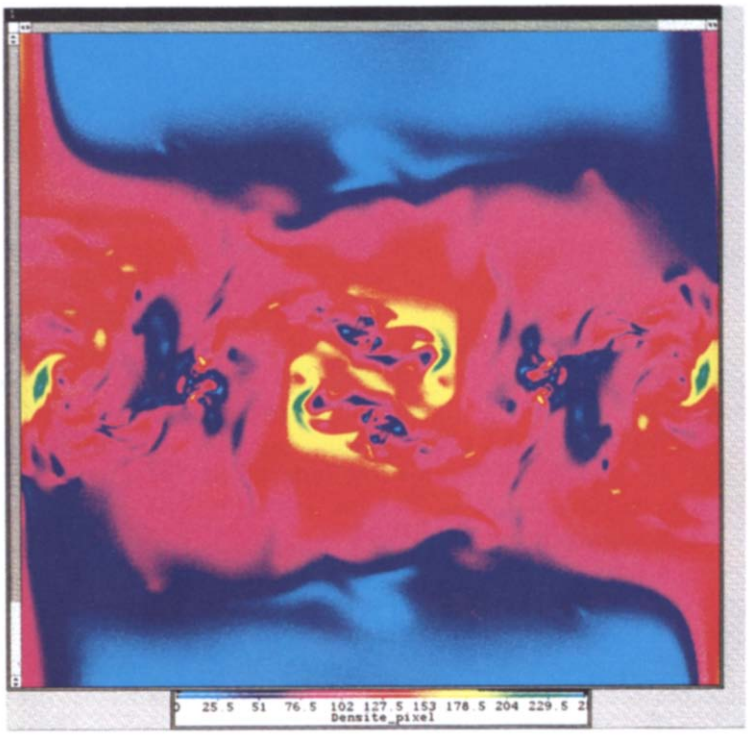

Fig. 6. Raster visualisation of the magnitude of velocity, shown as in figs. 3, 4 and 5. Because of the colormap we chose, the high-velocity regions appear in yellow. Note that these regions wrap around the vortex filaments.

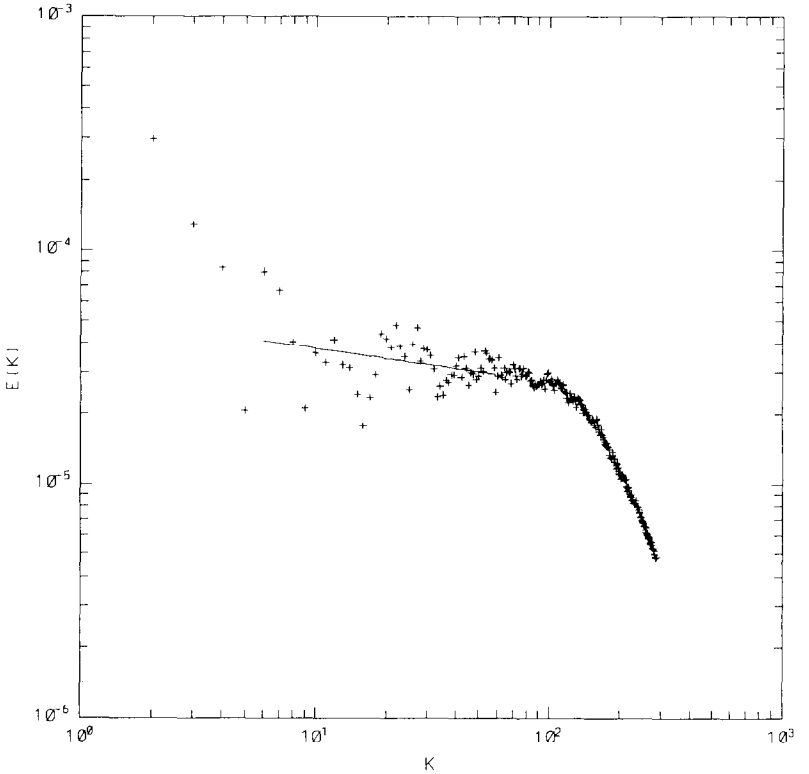

Fig. 7. Spectrum of vorticity fluctuations. The continuous line is a least-squares fit between $k = 6$ and $k = 60$ of the form $k^{-1+\mu}$ yielding $\mu = 0.86$.

We have tried to be more quantive about the relative concentration difference between the square of vorticity and the energy dissipation by measuring their intermittency via the spectra of their local fluctuations. Figures 7 and 8 show that these spectra follow power laws in $k^{-1+\mu}$ with $\mu = 0.38$ for the energy dissipation and $\mu = 0.86$ for the square vorticity. The exponent μ which was first introduced by Kolmogorov in 1962 [7] can also be interpreted as the Fourier fractal dimension of the dissipation in the limit of infinite Reynolds number [8]. Note that although some non-uniqueness of the exponent μ is taken into account in the multifractal theories of intermittency [9], these theories do not take into account the difference of exponent that we observe here beteween energy dissipation and square vorticity.

Another quantitative consequence of the stronger concentration of vorticity can be seen on fig. 9 which plots the probability distribution function of the pressure field at $t = 9$, for Reynolds numbers 1600, 3000 and 5000. The pdf is seen to be highly non-symmetric, with an exponential tail for negative pressures.

In summary our new results, obtained through direct numerical simulations, point to the existence of very strong depressions located on vortex filaments in fully developed turbulence. They also point to the fact that naive phenomenological theories that do not take into account the difference in scaling beteween ω^2 and σ^2 must be quite off the mark. Note that the experimental detections of the high-vorticity, low-pressure filaments has recently been possible in a fully developed turbulent flow by using cavitation in a liquid seeded with bubbles as a new visualization technique [10].

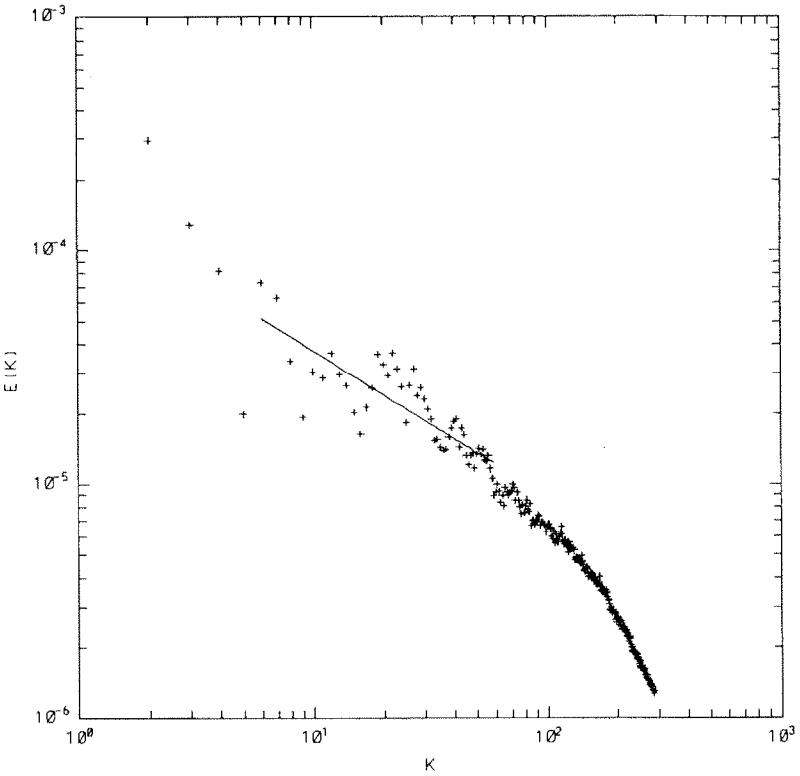

Fig. 8. Spectrum of energy dissipation fluctuations. The same fit as in fig. 7 yields $\mu = 0.38$.

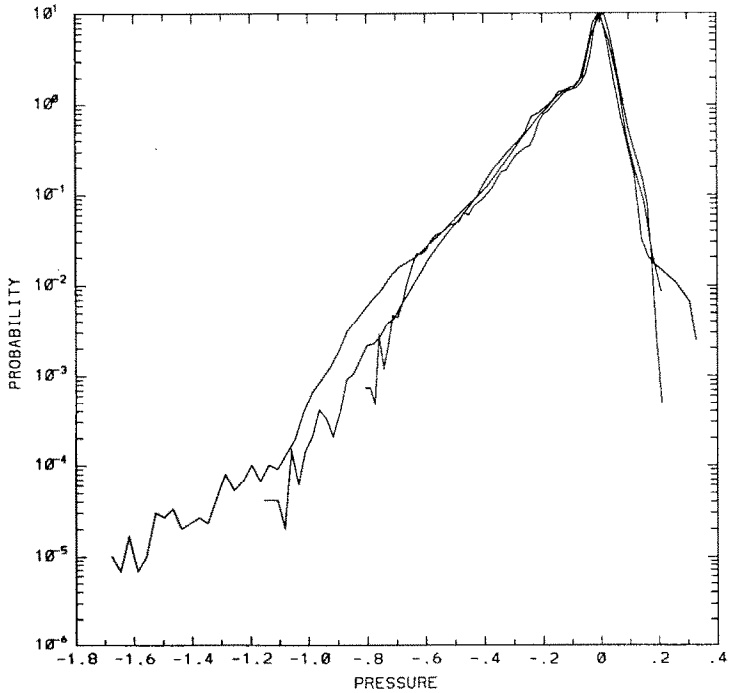

Fig. 9. Plot of the probability distribution function of the pressure field at $t = 9$, for Reynolds numbers 1600, 3000 and 5000. Note the long exponential tail for negative pressures corresponding to the vortex filaments.

The computations were done on the CCVR Cray-2 at Palaiseau, using the Fast Fourier Transforms of C. Temperton. The raster visualisations were performed with the help of DRET contract 87/1483.

References

[1] A.S. Monin and A.M. Yaglom, Statistical Fluid Mechanics, Vol. 2 (MIT Press, Cambridge, 1975).
[2] S.A. Orszag, in: Les Houches 1973, eds. R. Ballian and J.L. Peube (Gordon and Breach, London, 1977) p. 235.
[3] G.I. Taylor and A.E. Green, Proc. Roy. Soc. A 158 (1937) 499.
[4] D. Gottlieb and S.A. Orszag, Numerical Analysis of Spectral Methods: Theory and Applications (Soc. Ind. Appl. Math., Philadelphia, 1977).
[5] M. Brachet, D. Meiron, S.A. Orszag, B. Nickel, R. Morf and U. Frisch, J. Fluid Mech. 130 (1983) 411.
[6] A.N. Kolmogorov, C.R. Acad. Sci. URSS 30 (1941) 301.
[7] A.N. Kolmogorov, J. Fluid Mech. 13 (1962) 82.
[8] B. Mandelbrot, Turbulence and Navier–Stokes Equation, ed. R. Teman, Springer Lecture Notes in Mathematics 565 (Springer, Berlin, 1976) p. 121.
[9] G. Parisi and U. Frisch, Turbulence and Predictability in Geophysical Fluid Dynamics and Climate Dynamics, eds. M. Ghil and G. Parisi (North-Holland, Amsterdam, 1985) p. 71.
[10] S. Douady, Y. Couder and M. Brachet, Phys. Rev. Lett. to appear.